Graphene Multiplexed Sensor for Point-of-

Need Viral Wastewater-Based

Epidemiology

Michael Geiwitz^a, Owen Rivers Page^b, Tio Marello^a, Marina E. Nichols^a, Narendra Kumar^c, Stephen
Hummel^d, Vsevolod Belosevich^a, Qiong Ma^a, Tim van Opijnen^b, Bruce Batten^c, Michelle M. Meyer^b,
Kenneth S. Burch^{a*}

^a Department of Physics, Boston College, Chestnut Hill, MA 02467, USA

^b Department of Biology, Boston College, Chestnut Hill, MA 02467, USA

^c GRIP Molecular Technologies, Inc., 1000 Westgate Drive, Saint Paul, MN 55114, USA

^d Department of Chemistry and Life Science, United States Military Academy, West Point, NY 10996, USA

*Corresponding Author - Email: ks.burch@bc.edu (K.S. Burch)

Abstract

Wastewater-based epidemiology (WBE) can help mitigate the spread of respiratory infections through the early detection of viruses, pathogens, and other biomarkers in human waste. The need for sample collection, shipping, and testing facilities drives up the cost of WBE and hinders its use for rapid detection and isolation in environments with small populations and in low-resource settings. Given the ubiquitousness and regular outbreaks of respiratory syncytial virus, SARS-CoV-2, and various influenza strains, there is a rising need for a low-cost and easy-to-use biosensing platform to detect these viruses

locally before outbreaks can occur and monitor their progression. To this end, we have developed an easy-to-use, cost-effective, multiplexed platform able to detect viral loads in wastewater with several orders of magnitude lower limit of detection than mass spectrometry. This is enabled by wafer scale production and aptamers pre-attached with linker molecules, producing forty-four chips at once. Each chip can simultaneously detect four target analytes using twenty transistors segregated into four sets of five for each analyte to allow for immediate statistical analysis. We show our platform's ability to rapidly detect three virus proteins (SARS-CoV-2, RSV, and Influenza A) and a population normalization molecule (caffeine) in wastewater. Going forward, turning these devices into hand-held systems would enable waste-water epidemiology in low-resource settings and be instrumental for rapid, local outbreak prevention.

Keywords

SARS-CoV-2; Influenza; Respiratory syncytial virus; Graphene field effect transistor (GFET); Caffeine;
Aptamer

Introduction

According to the World Health Organization, lower respiratory infections are the fourth leading cause of death worldwide and second in low-income countries.¹ The top three causes for these infections are SARS-CoV-2, Influenza, and Respiratory Syncytial Virus (RSV).^{2–4} There is a growing emphasis on wastewater-based epidemiology (WBE) to track outbreaks. However, WBE is predominantly performed in high-income countries and densely populated areas.⁵ Furthermore, if detection can occur on site, WBE would be instrumental to mitigating and tracking outbreaks from these viruses via early detection of viruses and other pathogens shed by asymptomatic carriers without

requiring invasive and frequent individual tests. 6 For example, SARS-Cov-2 RNA can be detectable in wastewater 5 – 8 days before symptom onset and 2 – 4 days before positive clinical PCR tests. 7

Indeed, several college campuses exploited existing infrastructure to employ highly localized wastewater testing to prevent outbreaks during the Covid-19 pandemic. An instructive example is the University of California San Diego (UCSD), where sampling from 239 buildings across their campus allowed early hot spot detection and individual testing on a per-building basis. UCSD diagnosed nearly 85% of all SARS-CoV-2 infections on campus early and implemented preventative measures to mitigate the spread of the virus. This localized approach to WBE could also benefit low- and middle-income countries, where sewage is typically collected in individual or partially shared reservoirs that are not connected to community sewage systems. This is particularly relevant to RSV, a leading cause of respiratory-related deaths in those 0 – 5 years old where data from low- and middle-income countries is lacking or missing altogether due to inadequate systems and infrastructure needed to track disease transmission. Even in high-resource settings, the typical collection at a central waste-water facility limits sensitivity of pathogen detection in wastewater due to short half-lives of analytes of interest and natural dilution of target biomarkers.

Several factors have hindered the widespread adoption of WBE and led to the general reliance on sample collection at centralized treatment facilities. Specifically, WBE testing is performed almost entirely utilizing advanced techniques in analytical chemistry and molecular biology, including liquid chromatography-mass spectrometry (LC-MS), high-pressure liquid chromatography-mass spectrometry (HPLC-MS), digital polymerase chain reaction, or real-time quantitative polymerase chain reaction (RT-qPCR) that requires dedicated lab space, personnel, equipment, and chemicals. Limited testing facilities and the need for sample collection and transport can also delay results and response times, limiting WBE for effective outbreak prevention. Indeed, the WBE company BioBot in Cambridge, MA, says their average testing time is 11 – 15 days due to the need to test from multiple districts in weekly

batches, creating a sample testing backlog.¹⁶ Due to dilution of fecal waste in municipal wastewater, LC-MS and RT-qPCR rely on filtering and concentrating the collected sample^{17,18}, with HPLC-MS also subjecting it to several high-pressure steps to separate constituent elements.¹⁹ Thus, a low-cost, easy-to-use, multiplexed device is urgently needed to enable point-of-need WBE.

Particularly challenging is the need of a sensing platform to withstand the harsh wastewater medium while accurately and reliably distinguishing between the various components. Wastewater can contain viruses shed in human waste and other particles ranging from naturally occurring biomass, bacteria strains, and drug metabolites to pharmaceuticals. ²⁰ Similarly challenging is the need to multiplex assays or testing strategies to monitor multiple targets to reduce cost, time, and effort while addressing seasonal and population variations via normalization. For point-of-need WBE sensing, population normalization is crucial due to increased variability in dilution factors, such as per capita water use, stormwater inputs, *etc.*, and viral shedding rates. ²¹ This variability exacerbates the already challenging task of calculating the number of people infected based solely on the virus concentration in the wastewater sample. For example, depending on the level of infection, a person suffering from SARS-COV-2 can excrete anywhere from 600,000²² to 30,000,000 virions/L²³ of fecal matter.

To enable WBE at the local level, especially in low-resource and rural communities, it is helpful to look towards efforts in personalized health care. Substantial efforts have been made regarding sensing respiratory infections using lateral flow immunoassay (LFIA), low-cost PCR, and electronic sensors. Electronic sensors are potentially the most promising as they can simultaneously offer multiplexed, low-cost, high sensitivity detection with minimal human effort. Here, there is growing interest in graphene field effect transistors (GFET), which have shown the capability to detect everything from lead ions²⁴ to bacteria and oral disease biomarkers²⁵, though few have shown multiplexing capabilities.^{25–27} Nonetheless, only two groups, including ours, have demonstrated GFET's use for

detection of analytes in wastewater. For instance, a GFET recently detected cadmium ions in wastewater with a limit of detection (LOD) of 0.125 pM.²⁸

Graphene is particularly useful yet challenging as a transducer due to its extreme sensitivity to surface charges. ²⁹ Nonetheless, graphene is biocompatible and can be prepared at wafer scale. Due to its zero-band gap, it has a well-defined Dirac point (charge neutrality point) where its valence and conduction bands meet. This produces a peak in resistance when the chemical potential reaches the Dirac point (Figure 1a). When biomolecules attach to the surface of the graphene, it is generally assumed charge is transferred to graphene either directly or from conformal changes in the probe. ³⁰ This enables quantification of the target concentration via a shift in voltage at which the Dirac point appears.

Another advantage of graphene is the ease of functionalization with the biomolecules used as probes. These probes can be bonded to aromatic rings (*e.g.*, Pyrene), which attach to the graphene through π - π stacking. This allows for tremendous biocompatibility between graphene and a host of biomolecules without unintentional disorder from chemical bonding. However, typically, graphene is functionalized via a two-step process, where the linker molecule is attached using dimethylformamide (DMF), and then the probe is later bound to the linker molecule. Unfortunately, the DMF tends to react with the device, causing instability, higher LOD, and lower reproducibility, and can attack polymers and passivation layers, degrading the device. As described later, we have avoided this issue and improved the LOD and reproducibility needed for point-of-need WBE using probes pre-attached to the linker molecule and incubated in PBS.

Formatted: Not Highlight

Formatted: Not Highlight
Formatted: Not Highlight

Formatted: Not Highlight

Formatted: Not Highlight

Formatted: Not Highlight

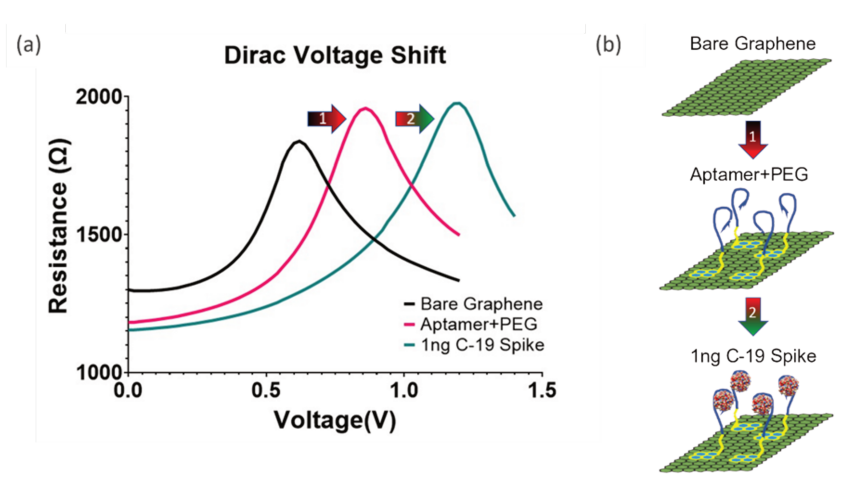


Figure 1 — Dirac voltage shifting with aptamer and target attachment: The numbered arrows in (a) and (b) correspond with each other and signify the steps in functionalization and sample testing. (a) The plot shows the positive shift in the Dirac point (peak of the curves) from the intrinsic position of the bare graphene (black) of approximately 0.6V. After a 2:1 mixture of the aptamer probe to PEG is added the Dirac point shifts positively to about 0.8V (pink). A large shift in the Dirac point to 1.2V is then seen (green) in the presence of Ing/ml of the target protein for SARS-CoV-2. (b) Schematic of the bare graphene, aptamer attachment, and target attachment.

Likewise crucial for detection in complex wastewater matrices, graphene is insensitive to the sample medium's pH levels. We demonstrated this in our recent work on opioid metabolite detection in wastewater. In which we showed the simultaneous detection of Noroxycodone, Norfentanyl, and EDDP (2-ethylidene-1, 5-dimethyl-3, 3-diphenylpyrrolidine) with an LOD below that of HPLC-MS. This work also exhibited our platform's robustness and selectivity of the target molecules in wastewater. Unlike traditional field-effect transistor (FET) sensors that require large gate voltages (>60 V). We have demonstrated our ionic liquid-gated GFETs are compatible with simple electronics requiring less than 2 V. 25,35

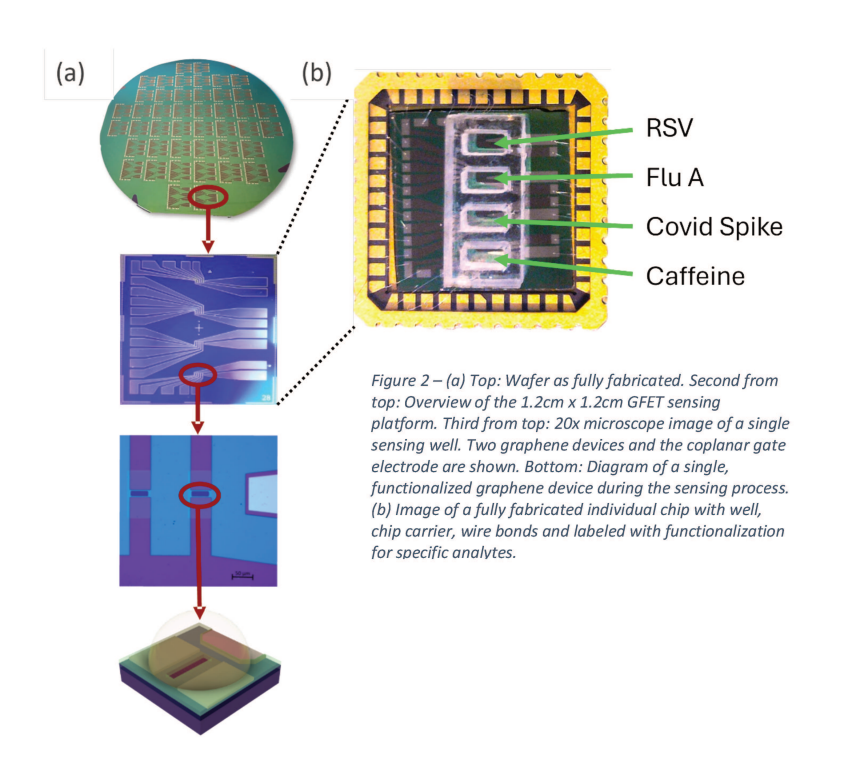
Still, virus protein detection in wastewater with GFETs, let alone by a scalable fabrication method, has not been shown. This work focused on developing wafer-scale fabrication of GFET devices for rapid, easy-to-use, low-cost, multiplexed, and population-normalized detection of respiratory viruses in wastewater at low levels of detection (LOD). To do so, we implemented a new probe strategy where

Formatted: Not Highlight

aptamers, single-stranded oligonucleotides, are pre-attached to the linker molecule, removing the need for harsh solvents in contact with the graphene devices. This enhanced the device's reproducibility, lowering dilution levels and producing better LOD. In addition, we have optimized the fabrication process to make forty-four chips simultaneously on a four-inch wafer. The devices are tested using freshly collected waste-water samples to detect SARS-CoV-2 Spike protein, Influenza A hemagglutinin, RSV glycoprotein, and caffeine for comparison with lab-based WBE methods.

Results and Discussion

GFET Manufacturing Improvements. To bring our GFET-based Graphene Electronic Multiplexed Sensor (GEMS) towards point-of-need WBE, we modified our fabrication method and device design to enable production on a four-inch silicon wafer (Figure 2a – Top) before dicing into individual chips. This



has significantly reduced our costs per chip primarily due to a drastic decrease in fabrication time. Prior to wafer-scale fabrication, we were able to produce 6 – 8 chips in four days. We can now produce forty-four GEMS in the same amount of time. Each GEMS has 20 GFETs arranged in groups of five for rapid statistical analysis of variability between GFET devices. To enable multiplexed detection, the groups are segregated with PDMS wells with individual coplanar side gates (Figure 2b). This enables individual functionalization of each well with a different probe without cross-functionalization.

Pre-Linked Aptamers. We employ aptamer probes due to their high affinity, stability, and small size. ³⁶ Aptamer-based protein biosensing depends on aptamer-target binding ³⁷, which several factors can complicate. Structurally complex protein targets have more binding sites and interaction types than small molecules. ³⁸ This increase in complexity can result in aptamers with decreased target specificity if the experimental design of SELEX is flawed. ³⁹ Generation of aptamers for proteins via SELEX is more manageable for small molecules ³⁷, but the conformation of the protein (purified or native) can alter or hinder aptamer binding. ⁴⁰ Careful consideration is necessary to ensure binding conditions mirror realworld binding conditions. With this in mind, we chose the Universal Aptamer (UA) ⁴¹ for Influenza A hemagglutinin, H8⁴² for RSV, and 1C⁴³ for SARS-CoV-2 Spike proteins based on their binding affinities to their targets. See *Supporting Information* S7 for further information regarding the aptamers.

Generally, to attach the aptamer to graphene, the device is first incubated with 10 mM 1pyrenebutyric acid N-hydroxysuccinimide ester (PBASE) linker molecule dissolved in DMF for one hour.

After performing a Dirac point measurement to see the shift due to DMF and PBASE, a 2:1 mixture of aptamer to polyethylene glycol (PEG) is incubated for one hour. Adding PEG to the probe mixture has been widely employed⁴⁴ to prevent unwanted attachment of molecules to any unlinked PBASE molecules and provide space between aptamers, limiting their interactions. The PEG also stabilizes the devices by minimizing drift and standard deviation between different devices.

To further reduce cost, analysis, and fabrication time and boost reproducibility, we altered this typical process by pre-attaching the aptamers and PEG to the PBASE molecules (See Figure S8 for more details regarding pre-linking.). This has allowed us to avoid DMF contact with the graphene devices.

While the exact mechanism is not clear, previous studies have shown DMF can dope graphene by acting as an electron donor. The excess electrons are not easily removed from the graphene and thus affect the device's limit of detection. With this in mind, we performed identical experiments with GEMS using the standard DMF attachment procedure and our pre-linked PEG (PL-PEG) and probes (PL-aptamers). As seen in Figure 3 and Table 1, more significant Dirac point shifts occurring at much lower LODs are seen in devices with pre-linked (PL) probes. Lastly, to ensure graphene cleanliness and device reproducibility, much of the fabrication was carried out in a pure argon environment inside our cleanroom-in-a-glovebox. 46

Optimization in PBS – Viral protein aptamers. Selectivity and concentration analysis was first conducted in 1x PBS to determine the aptamer viability without the background signal from wastewater. Specifically, the numerous constituent components in wastewater⁴⁷, many of which are charged ions, can produce false positives. For each target, we first determined the initial Dirac point of the graphene in 0.01x PBS (see Figure S2). Diluted PBS minimizes the Debye screening effect.⁴⁸ Typically, we observe a Dirac point around $0.6 \text{ V} (\pm 0.1 \text{ V})$ due to the work function of the platinum side gate electrode ⁴⁹. This baseline Dirac point ensures the graphene quality without unwanted doping. This is further confirmed by the nearly symmetric slopes to the left (hole regime) and to the right (electron regime) of the Dirac point, which results from the charge carrier mobilities.⁵⁰ Passivation issues are typically indicated by double-peaks in the curves. Good passivation is also confirmed by ensuring the Dirac point does not drift with repeated gate voltage sweeps. The highest quality devices have an initial Dirac point in the range of 0.58-0.7 V with an average starting resistance around 2000Ω and a stable Dirac point after three measurements. Data on initial Dirac point and starting resistances were collected for 545 different

Formatted: Not Highlight

Formatted: Not Highlight

GFETs fabricated over two years in our lab, showing that most of our devices fall within these parameters (see Figure S3).

After initial testing, we incubated the graphene devices for one hour with a 2:1 mixture of 10uM PL-aptamer to 10uM PL-PEG, which was optimized in our previous work with opioids in wastewater and oral disease biomarkers in saliva. ^{25,27,35} Dirac point measurements are again conducted in 0.01x PBS to confirm attachment to the graphene surface. Upon attachment, the charged phosphate backbone of the aptamer induces positive charge carriers into the graphene, producing a positive 150-200mV shift in the Dirac point (see Figure S2). Atomic force microscopy and Raman measurements have also been performed to confirm the attachment (see Figures S5 and S6).

We first assessed all aptamer selectivity against a negative control. For example, Influenza A hemagglutinin (HA) with a concentration of 10-100 ng/ml that is far beyond that found in wastewater (tens of pg/ml), is incubated on the devices for one hour in the well containing the SARS-COV-2 Spike protein aptamer (1C). No shift in the Dirac point was seen, showing the HA protein does not bind to the 1C aptamer (Figure 3 – Covid). Similar negative control analyses were conducted in the wells functionalized with the Influenza and RSV aptamers. As shown in Figure 3, these aptamers had a slightly higher non-specific interaction with the negative control proteins. Nonetheless, the Dirac point shifts in wells with the Influenza and RSV aptamers resulting from negative controls were relatively small (approximately 50 mV), setting the baseline for future measurements.

Next, we focused on assessing each aptamer's limit of detection and affinity. We followed a standard protocol of incubating the devices with a specific concentration of the target proteins. After incubation, the device is rinsed with 1x PBS and DI water before performing the Dirac point measurement in 0.01x PBS. For each concentration, the reported shift is the difference in the Dirac point value obtained from that of the negative control. After measuring the Dirac shift, we incubated with

increasing target protein concentrations. To ensure the absence of systematic errors, we have also performed measurements with random concentrations to ensure they match the signal detected by a systematic increase in concentration.

Beginning with low concentration, each incubation is conducted for one hour. We found that concentrations below 1 fg/ml for the SARS-COV-2 Spike protein did not change the Dirac point.

However, the RSV and HA proteins produced shifts at much lower concentrations (approximately 10 ag/ml). This shift discrepancy may be due to the newness of the SARS-COV-2 Spike aptamer and future improvements can improve its binding affinity. The average shift from all devices in the well and their

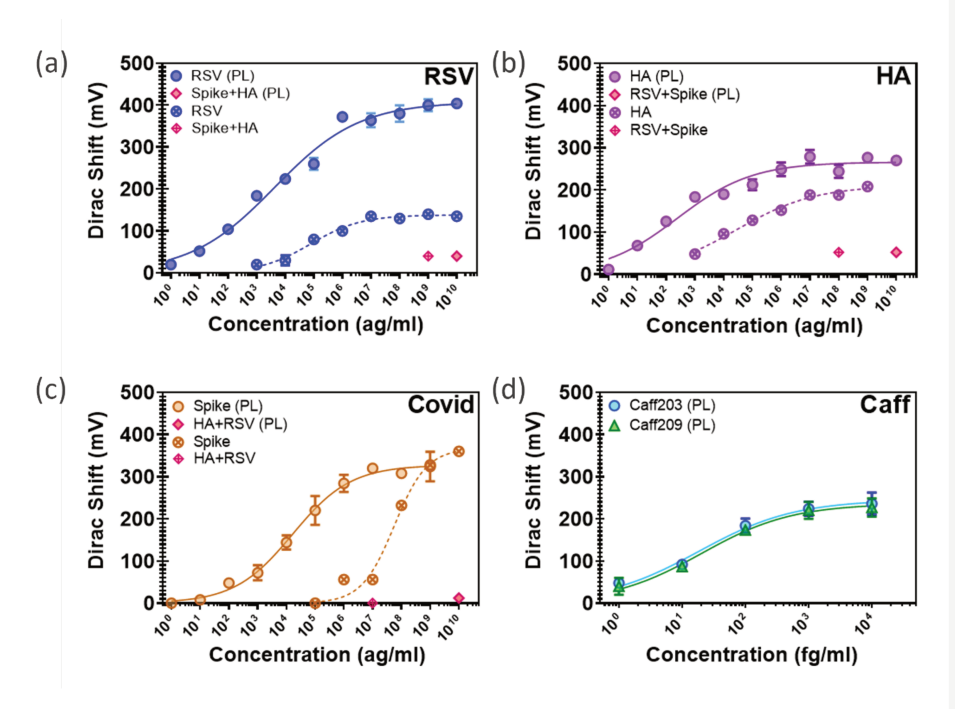


Figure 3 – Concentration dependance measurements of viral proteins in PBS. Error bars calculated from the five GFETs per sensing well. Data points with crosses and dashed curves indicate non-pre-linked aptamers were used. (a) RSV detection. High concentrations of HA and COVID Spike proteins used as a negative control. (PL) denotes pre-linked aptamer experiment. (b) and (c) Same as in RSV plot but with SARS-COV-2 Spike and RSV proteins, respectively. Non-target proteins used as negative control in each case. (d) Concentration dependence measurements of two caffeine aptamers. Caffeine measurements were only conducted with pre-linked aptamers.

standard deviations are plotted in the same graph as the negative control's shift. The concentrations are increased by one order of magnitude in each subsequent incubation, and the same rinsing and sensing protocol is conducted for each. The concentrations are increased until a saturation point is reached, determined by no further shift with two consecutive high concentrations.

Upon collecting the concentration dependence, we found the binding characteristics of the aptamer by fitting the Dirac voltage shift versus target analyte concentration to Hill's equation⁵¹:

$$V_D = \frac{V_D^{max} * C^n}{K_D^n + C^n} \tag{1}$$

Here, V_D is the Dirac voltage shift measured in mV, V_D^{max} is the maximum Dirac voltage shift at the saturation point, C is the concentration of the target analyte, n is the Hill Coefficient determined to be the maximum slope on a log plot of the response curve, and K_D is the dissociation constant. The parameters were found using a least squares fit model in Matlab after providing estimates of the Hill Coefficient, maximum Dirac voltage, and dissociation constant. Due to the five devices in each well of the GFET, we can perform statistical analysis immediately. This allows us to calculate the LOD for each analyte by using the residuals of the standard deviation against the Hill fit using 3σ analysis⁵²:

$$LOD = \frac{3\sigma}{n} \tag{2}$$

Here, σ is the standard deviation from the fit and n is again the Hill slope. This was used to find the LODs in Table 1.

Table 1 Comparison of LODs between pre-linked and unlinked aptamers for each target analyte in PBS. All pre-linked virus experiments were conducted on a single GFET chip and unlinked on another. Caffeine experiments were only performed with pre-linked aptamers and done on a single GFET chip.

Target	Unlinked Aptamer	Pre-Linked Aptamer	
SARS-CoV-2 Spike Protein	91 pg/ml	55 ag/ml	
Hemagglutinin (Flu A)	79 fg/ml	408 ag/ml	
Respiratory Syncytial Virus Protein	43 fg/ml	453 ag/ml	
Caffeine	N/A	Caff203: 35 fg/ml Caff209: 26 fg/ml	

Caffeine aptamer. WBE programs use several different biomarkers to determine the total contributing population. These include caffeine, paraxanthine (caffeine's metabolite), creatine, 5-hydroxyindoleacetic acid (5-HIAA, serotonin metabolite), and pepper mild mottle virus (PMMoV) given their ubiquitousness in human diets and survivability in wastewater. To the best of our knowledge, no aptamer has yet been developed for PMMoV or paraxanthine. Therefore, to test our platform's capabilities as a means for population normalization in wastewater, two previously reported caffeine aptamers were selected based on their reported results that show micromolar sensitivity in human serum 4, two of which (Caff203 and Caff209) were chosen for our tests in wastewater. Both the Caff203 and Caff209 aptamers were pre-attached to the PBASE linker molecules, and the same functionalization and sensing protocols were followed as the virus proteins. Both were evaluated first in PBS to determine their viability before exposure to wastewater. Caff203 was found to have an LOD of 35 fg/ml in PBS, while Caff209 showed 26 fg/ml in PBS (Figure 3). Due to its lower LOD, Caff209 was selected for future experiments.

Wastewater biosensing – Wastewater dilution optimization. Next, we turned to testing GEMS with wastewater. In our earlier work on opioid metabolites, we found diluting the wastewater with 1x PBS to a 20:1 mixture necessary to minimize unwanted Dirac point shifts and false positives from the

myriad components and non-neutral pH (6-9). Given the improved device performance with preattachment, we re-optimized this dilution to attempt a lower LOD. We began by incubating the 1C PLaptamer and PL-PEG, as previously discussed. The wastewater was then passed through a 0.3-micron
filter to remove large particulates. Next, various dilutions (2:1, 5:1, 10:1, and 20:1) were incubated
directly on the devices for one hour, and the resulting Dirac point shift is shown in Figure 4. We found
the 10x dilution caused an approximate 60 mV Dirac point shift, the same as the 20x dilution. Since PBS
does not induce a shift, the background signal from wastewater will increase the LOD by setting a floor
below which we cannot uniquely detect the target, as indicated by the horizontal dashed lines in Figure
5. Next, four samples were diluted with the 2:1, 5:1, 10:1, and 20:1 PBS to wastewater samples to create
1 ng/ml solutions of SARS-COV-2 Spike protein and incubated on the devices for one hour. This was
done to determine if wastewater dilution affected the ability of the aptamers to find the target proteins.
The 1 ng/ml concentration was used since this is the point at which the SARS-COV-2 Spike protein
aptamer saturated when tested in 1x PBS. Interestingly, there was a statistically insignificant difference
in the shift between the 10:1 and 20:1 wells. Both measured a shift of around 130 mV after incubating

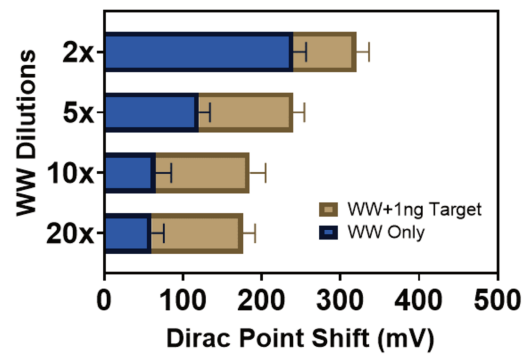


Figure 4 – Histogram of the average Dirac point shift at various wastewater dilutions. The blue areas show the average Dirac point shift for five GFET devices after incubation of diluted wastewater for one hour. The tan areas show the further Dirac point shift after incubating the GFETs for one hour with 1ng/ml of target protein in their respective wastewater dilutions.

with the Spike protein mixture. Thus, we focused 10:1 PBS to wastewater dilution to achieve the smallest possible LOD in wastewater.

a similar series of concentration-dependent measurements with the same protocol done first in PBS.

The experiments were conducted in two rounds for each analyte. Experiments were first performed on a single GFET chip. Four wells were functionalized with a different pre-attached aptamer: 1C for SARS-CoV-2 Spike protein, UA for Influenza A hemagglutinin, H8 for RSV glycoprotein, and Caff209 for caffeine. A fresh wastewater sample was obtained (collected one day prior and stored a 4°C overnight), filtered, and diluted in a 10:1 ratio with PBS and spiked with virus proteins and caffeine to make concentrations ranging from 1 fg/ml to 1 ng/ml with an increase of one order of magnitude between each concentration. The second round of experiments was conducted one month later using a newly fabricated GFET chip, fresh pre-attached aptamers, and a new wastewater sample. In both instances, the negative controls were tested first at 1 ng/ml to check selectivity, followed by increasing the concentrations of the target analyte. In both rounds, the negative controls showed little to no shift beyond the background 60mV shift from the wastewater (dashed lines in Figure 5).

The resulting concentration curves are shown in Figure 5, and LODs for each round are shown in Table 2. As expected, LOD values increased over the PBS results due to the intrinsic 60mV signal from the wastewater. Nonetheless, the larger LODs are all well within the range for the concentrations of each analyte in wastewater. SARS-CoV-2 has been shown to contain 24±9 Spike proteins per virion⁵⁵, theoretically suggesting the LOD for our GEMS platform to be on the order of 27 – 59 virions/ml (27,000 – 59,000 virions/L) in wastewater assuming fully lysed virions. Influenza A has been found to contain 300 – 400 HA proteins per virion⁵⁶, giving a theoretical LOD of fully lysed virions in the 1.5 – 7 virions/ml (1,500 – 7000 virions/L). To the best of our knowledge, the average number of proteins for RSV has not yet been determined. Assuming a similar number between the Spike and the Influenza A proteins, the

theoretical, fully lysed RSV virions could be 15 – 397 virions/ml (15,000 – 397,000 virions/L). Like the experiments conducted in PBS, the RSV and SARS-COV-2 Spike aptamers show little to no shift with the high concentration of negative control. In contrast, the HA aptamer showed a small but significant shift of around 60 mV with negative control. This could be partly due to UA's longer length compared to the others, allowing it to bind to more constituent elements in the wastewater. It could also be due to HA proteins already present in the wastewater sample, which was collected during the 2022 – 2023 Flu season. We additionally tested each of the virus proteins in a different wastewater source with similar result shown in Figure S9.

Formatted: Not Highlight

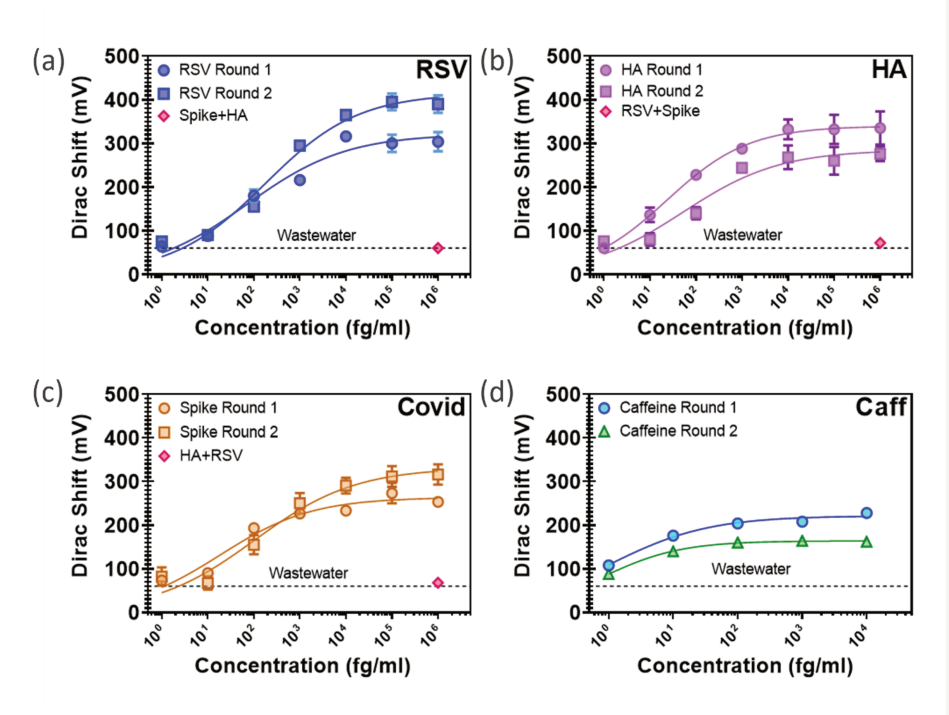


Figure 5 – Concentration dependence measurements of viral proteins and caffeine in wastewater. Error bars calculated from the five GFETs per sensing well. (a) RSV; (b) HA; (c) COVID spike proteins; and (d) Caffeine. Horizontal dashed line shows intrinsic background shift from the wastewater itself.

Due to its lower LOD found in PBS (Table 1), Caff209 was selected for analysis in wastewater.

Interestingly, the LOD in wastewater was lower than in PBS, which was not seen with the virus proteins.

This could be due in part to the salt content in wastewater facilitating binding ⁵⁷ of the much smaller caffeine molecules, which are 0.194 kDa as compared to the larger proteins having sizes of 139.7 kDa, 59 kDa, and 37 kDa for Spike, HA, and RSV respectively, lowering the variability between the devices.

Noting that GEMS generally achieves LODs for the three viruses studies of 100-200 fg/mL in wastewater, we now compare these LODs with those reported for lab-based techniques. For LC-MS, a variety of studies have found LOD 3000 fg/mL for SARS-CoV2 in nasopharynx samples, 65,66 and reported detection at X concentration in wastewater. 69 In addition, LC-MS LOD's for Influenza A hemagglutinin. 67 are 30,000 fg/mL and for RSV are 40,000 fg/mL67. Thus GEMS has a one to two order of magnitude better LOD than LC-MS. A much better LOD of X has been achieved via RT-qPCR58; however, similar to LC-MS, this requires a lab setting to perform the concentration and additionally relies on amplification requiring complex machinery and chemicals. Similarly, an LFIA sensed human adenovirus in processed wastewater by first concentrating the wastewater sample through PEG precipitation overnight and then performing a recombinase polymerase amplification step and achieving an LOD of 50 copies/reaction starting from an initial sample size of 1 L.70

These amplification techniques provide impressive LOD, but they do not sense proteins (i.e., caffiene) needed for population normalization and come at the cost of long lead times, the need for a lab and human collection. This has driven the reliance on sampling at central facilities, where the concentrations are far diminished due to dilution and virus decay. Indeed, the LODs are far lower than the shed virus levels ranging from $10^2 - 10^7$ copies/ml. 63,64 Thus, beyond fast turnaround and low cost, more localized collection and analysis also bring the benefit of not requiring such low LODs. To the best of our knowledge, the only other option are so-called "rapid tests" based on LFIA. However these have not shown the ability to rapidly sense the low level of virus in unprocessed wastewater. A summary

Deleted: To put these LODs in context, we

Deleted: m

Deleted: other

Deleted: LODs

Formatted: Not Highlight

comparison comparison between the dynamic ranges, analysis time, LODs and estimated cost for PCR,

LC-MS, LFIA, and GEMS is shown in Table 2.

Table 2

Comparison of dynamic range, testing time, limits of detection (LOD) in wastewater, and cost for various platforms. Costs are reported for a novice user who would like to have their own samples analyzed.

<u>Platform</u>	<u>Dynamic Range</u>	<u>Testing Time</u>	LOD in Wastewater	Estimated Cost
Our GFET	1 ag/ml – 10 ng/ml	<u>20 – 40 minutes</u>	<u>2 – 200 fg/ml</u>	~\$15/chip
<u>LFIA</u>	$10^5 - 10^6 \text{ copies/ml}^1$	5 – 30 minutes ¹	None reported for these viruses in wastewater	~\$20
<u>PCR</u>	1 – 100 copies/ml ¹	11 – 15 days ^{3*}	9 copies/ml ⁴	Kit: \$120 Testing: not reported, must receive quote ⁵
LC-MS	$10^3 - 10^7 \text{ copies/ml}^6$	~8 hours for three compounds ⁷	$10^6 - 10^7 \text{ copies/ml}^6$	\$1130

wastewater source and performed a blind test with the original wastewater. First, we note that the tests performed throughout the paper primarily include samples taken from Joint Air Base Cape Cod but were collected in June of 2023 (Figure 5, "Round 1" curves) and February of 2024 (Figure 5, "Round 2" curves). To confirm the robustness of the device, a second set of tests were performed with wastewater collected from Veolia wastewater treatment facility in Westborough, MA in May of 2024. We note the two sources serve substantially distinct populations; nonetheless similar results were obtained (Figure S9). We performed blind tests using a single chip functionalized with each virus aptamer in a different well. Four concentrations of each target protein were made by one author (O.R.P.) and were coded with a four-digit number (1738, 1993, 2930) with no indication of the contents. These were tested by another author (M.G.) using the same sensing protocol outlined above to determine which coded sample contained each protein. As shown in Figure 6, for concentrations above 100 pg/mL (consistent with our

Formatted: Not Highlight

Deleted: BioBot reports a limit of detection (LOD) for SARS-CoV-2 of 9000 copies/L using RT-qPCR⁵⁸ (approximately 10 whole virions/L), which is lower than concentrations typically found in wastewater. The reliance on lab testing results from these low virus loads in wastewater requires amplification and/or viral concentration steps to detect. These concentrations can range from, in the case of SARS-CoV-2, 150,000 - 141.5 million viral genome copies (150 -141,500 whole virions⁵⁹) per liter of wastewater.⁵ Influenza A concentrations are reported to be around 260,000 copies per liter⁶⁰ and RSV 1,071 – 70,700 copies per liter.⁶¹ Others have reported LODs from RT-qPCR as low as 2.9 - 4.6 copies per reaction after concentrating the sample from 50 ml to $20~\mu l.^{62}$ Several studies have found levels of shed virus can vary substantially depending on patient infection level and virus variants, ranging from $10^2 - 10^7$ copies/ml. 63,64 These levels will significantly decrease upon reaching a wastewater treatment facility due to dilution and virus decay, highlighting the need for more localized collection and analysis. While our GEMS platform cannot achieve the low LODs seen with RT-qPCR, its LODs are 1 – 2 orders of magnitude lower than what has been reported with LC-MS (Table 2).

Formatted: Font color: Auto

Commented [KB1]: make same LOD units and add sentence from old table about how converted from copies to fg

Deleted: Limits of Detection (LOD) for each target analyte from two separate experimental rounds. Each round was conducted on a single GFET chip. Based on their average molecular weights, LODs were converted from fg/ml to proteins/ml.

Commented [KB2]: not really true should report the actual time but include the preparation work... this is just biobot

earlier LOD) the target can easily be identified by only producing a Dirac shift in one well. Based on this,

M.G. identified each target, which was confirmed accurate by O.R.P.'s written records.

Conclusions and Future Work

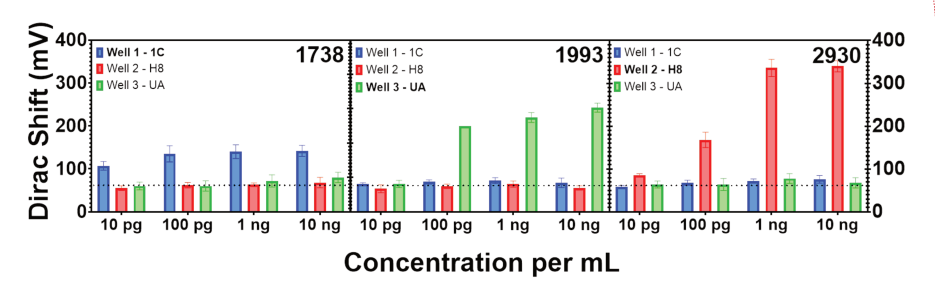


Figure 6 – Wastewater Blind Tests: Each plot represents the differing concentrations for a coded sample. The assorted colors indicate the aptamer used in each well; blue for the 1C (Covid), red for H8 (RSV), and green for UA (Flu). The horizontal dotted line is the intrinsic shift from the wastewater. M.G. found that 1738 was COVID spike proteins (left), 1993 was HA (middle), and 2930 was RSV. Each was confirmed by O.R.P.'s written records.

To summarize, we showed the viability of our GEMS platform for selective, specific, simultaneous, and highly sensitive detection of four different analytes in wastewater, including caffeine for population normalization and three different viral proteins. We achieved limits of detection (see Table 1) one to two orders of magnitude better than HPLC-MS (Figure 5)^{65,66,69} and below the levels needed for effective early interventions. ⁶⁹ Results are obtained using a 1 cm² chip in just over one hour with minimal human intervention and without bulky, expensive lab equipment or costly reagents. Simple wastewater preparation can be easily performed with minimal training, while low voltage and resistance ranges can be operated with simple and cheap electronics. The cost is minimized by wafer-scale fabrication and pre-linked aptamers, further enhancing reproducibility and LOD. Combined with our previous results, the scalable GEMS platform enables rapid, easy, and cheap wastewater sensing of a wide range of analytes (opioid metabolites, viruses, *etc.*). This shows our platform to be a practical choice for wastewater-based epidemiology for viral testing and can lead to finding hotspots for future

Deleted: In the case of LC-MS, LODs between 105 - 106 copies per nasopharynx sample^{65,66} (approximately 3000 fg/ml) have been reported. For SARS-CoV-2 spike proteins in wastewater, we achieved an LOD of 136 - 187 fg/ml, which is an order of magnitude lower than achieved by LC-MS in nasopharynx samples. To the best of our knowledge, while LC-MS has been used to detect SARS-CoV-2 in wastewater⁶⁹, no detection limit has yet to be reported. Even more pronounced, we find an LOD of 39.6 - 181 fg/ml for Influenza A hemagglutinin, which is two orders of magnitude lower than the reported LOD of LC-MS (30,000 fg/ml).67 Similarly, our LOD of 176 fg/ml for RSV in wastewater is also two orders of magnitude lower than LC-MS value of 40,000 fg/ml. 67 So-called "rapid tests," on the other hand, while having short analysis time, typically rely on LFIA, which to the best of our knowledge have not shown the ability to rapidly sense the low level of virus in unprocessed wastewater. An LFIA sensed human adenovirus in processed wastewater by first concentrating the wastewater sample through PEG precipitation overnight and then performing a recombinase polymerase amplification step and achieving an LOD of 50 copies/reaction starting from an initial sample size of 1 L.70 While this is a low LOD, the tradeoff is in the time and complexity of the analysis. A comparison between the dynamic ranges, analysis time, LODs and estimated cost for PCR, LC-MS, LFIA, and our GFET devices is shown in Figure S10.

Formatted: Not Highlight
Formatted: Not Highlight

virus outbreaks. Our platform's low cost and power requirements could allow WBE to be performed on a building-by-building level in low-resource or rural settings, ushering in a new era of wastewater testing. Enabling this will require future efforts for on-chip electronics and microfluidics for sample preparation and a more comprehensive array of analytes to be tested on the same chip.

Materials and Methods

Materials. The aptamers (Caff209, 1C, Universal Aptamer, and H8) were chemical synthesized in a 5'-amine-sequence-3') configuration by Integrated DNA Technologies (IDT), Coralville, IA. The 1C, 4C, and UA sequences were modified to an unpaired 5'-end nucleotide tail for amine attachment. The SARS-CoV-2 Spike protein biotinylated (SPN-C82E9), and RSV glycoprotein (RSG-V5221) were purchased from ARCO Biosystems while the biotinylated Hemagglutinin (HA) protein (11085-V08H-B) was obtained from Sino Biological. PBASE, DMSO, and PEG were obtained from Sigma-Aldrich. DI water, PDMS, and IPA were obtained from Fisher Scientific. The influent wastewater samples were obtained from MASSTC in Sandwich, MA. To avoid biofouling, wastewater samples were passed through a 0.3-μm filter and diluted 10:1 binding buffer (1x PBS + 2mM MgCl₂ + 1% methanol) to wastewater. These dilutions were then used to create various concentrations of virus protein and caffeine concentrations. The dilution steps were performed to enhance cooperative binding between aptamer and target analytes. The dilutions have been accounted for when calculating LODs to ensure the concentrations mirror the original sample.

GFET Fabrication and Characterization. We first pattern bottom contacts on a four-inch Si/SiO_2 wafer using bi-layer photoresist (LOR1A/S1805) and photolithography followed by e-beam deposition of 5 nm of titanium wetting layer and 20 nm of platinum. Platinum is chosen to minimize contact resistance to graphene because it is robust and has low surface potential.⁴⁹ After metal liftoff, the contacts were annealed under vacuum for 10 hours at 400° C to remove any remaining photoresist and

transferred on top of the entire wafer by General Graphene Corp. in Knoxville, TN. The wafer was then annealed under vacuum in the e-beam chamber for nine hours at 300°C to remove any remaining residues and water from the transfer process. Before removing from the e-beam chamber, 3 nm of aluminum oxide (AlOx) was deposited to protect the graphene from further chemicals and atmosphere during later fabrication steps. Once removed, the wafer was baked on a hotplate in our glovebox at 175°C for five minutes to ensure aluminum oxide adhesion. The same bi-layer resist process and photolithography system were then used to pattern the graphene for etching via oxygen plasma. The MF-321 developer (from Kayaku) used to develop the pattern after lithography has the added benefit of also removing the 3 nm of AlOx from atop the graphene we wish to etch. This was followed by argon plasma to remove any oxide layer formed on the platinum by the oxygen plasma on the coplanar side gate. Failing to remove this layer has led to higher initial Dirac points and, in turn, lower sensitivity in our devices.

Next, the devices were cleaned with Remover PG and rinsed with IPA and DI water. The chips were then baked under a vacuum at 200°C for one hour to remove any water and clean any residue from the wafer. After this, a 50 nm passivation layer of aluminum oxide was deposited to encapsulate the devices while the wafer was still hot. Oxygen was flowed to achieve a pressure of ~10⁵ Torr during AlOx deposition to replenish oxygen stripped from the AlOx crystals during e-beam deposition. A final single layer (S1805) photolithography step was then performed to expose the graphene sensing windows (10um x 40um) and the contact pads for wire bonding. Exposed AlOx was then etched with 65:35 diluted TRANSETCH-N (from Transene) for 14 minutes at 80°C, then rinsed with DI water. The remaining photoresist was then removed with Remover PG and rinsed with IPA and DI water. The wafer was then diced using a Pelco Wafer Dicing system, eliminating the need for a wafer dicing saw and its associated chemicals. The chips were then mounted to chip carriers and wire-bonded. Following this,

PDMS wells made in-house with custom 3D-printed molds were placed on the chips to hold the functionalization liquids and target mixtures during incubation as per our sensing protocols.

GFET Functionalization and Measurements. The *in vitro* pyrene-aptamer conjugation differs from the previous linking reaction²⁷ in that it was performed in a microcentrifuge tube instead of on the graphene surface. The goal of this acyl transfer is for the NHS ester group of the 1-Pyrenebutyric acid N-hydroxysuccinimide (PBASE) to interact with the amine group attached to the 5' end of the aptamer (S8a), resulting in a pyrene-linked aptamer that can be attached to the graphene. See *Supporting Information* for further details regarding pre-attachment. Each GFET well was functionalized with a 2:1 mixture of the different pyrene-linked aptamers to PEG for and optimized time of one hour at a concentration of 10 mM. This concentration was found to ensure maximum graphene area coverage. The chips were then rinsed with 1x PBS to remove excess aptamer and PEG, then rinsed with DI water to remove excess salts from the graphene surface. For analyte detection, 40 minutes of incubation at each target concentration was found to be optimal and utilized for all experiments.

Author Information

Corresponding Author

Kenneth S. Burch – Department of Physics, Boston College, Chestnut Hill, Massachusetts 02467, United States; orcid.org/0000-0002-7541-0245; Email: ks.burch@bc.edu

Authors

 $\label{lem:michael Geiwitz-Department of Physics, Boston College, Chestnut Hill, MA 02467, United States; orcid.org/0009-0000-7197-9381$

 $Owen \ Rivers \ Page-Department \ of \ Biology, \ Boston \ College, \ Chestnut \ Hill, \ Massachusetts \ 02467, \ United States; \ orcid.org/0000-0003-4072-8509$

Tio Marello – Department of Physics, Boston College, Chestnut Hill, MA 02467, United States

Marina E. Nichols – Department of Physics, Boston College, Chestnut Hill, MA 02467, United States; orcid.org/0009-0006-4355-809X

Narendra Kumar – GRIP Molecular Technologies, Inc., 1000 Westgate Drive, Saint Paul, MN 55114, United States; orcid.org/0000-0002-5319-1547

Stephen Hummel – Department of Chemistry and Life Science, United States Military Academy, West Point, NY 10996, United States

Vsevolod Belosevich – Department of Physics, Boston College, Chestnut Hill, MA 02467, United States

Qiong Ma – Department of Physics, Boston College, Chestnut Hill, MA 02467, United States

Tim van Opijnen – Department of Biology, Boston College, Chestnut Hill, Massachusetts 02467, United States

Bruce Batten – GRIP Molecular Technologies, Inc., 1000 Westgate Drive, Saint Paul, MN 55114, United States

Michelle M. Meyer – Department of Biology, Boston College, Chestnut Hill, Massachusetts 02467, United States; orcid.org/0000-0001-7014-9271

CRediT authorship contribution statement

K.S.B., M.G., and N.K. conceived the project and designed the experiments. M.G. fabricated, functionalized, and tested all GFET platforms. M.G., N.K., S.H, T.v.O., and K.S.B. selected all aptamers and analyzed the data. O.R.P. pre-linked all aptamers with PBASE linker molecules. T.M. aided in the design and placement of PDMS wells. S.H. validated 1C aptamer with flow cytometry. V.B. performed AFM and wire bonding machine maintenance. Q.M. supervised AFM and wire bonding maintenance. T.v.O. supervised flow cytometry. M.M. supervised aptamer pre-linking and blind test sample preparation. B.B. and K.S.B. aided in data analysis. M.G., O.R.P., and K.S.B. wrote the manuscript.

Data Availability

All data is available on request.

Acknowledgements

The work of M.G., T.M., M.E.N and K.S.B. are grateful for the support of the National Science Foundation (NSF) EPMD program via grant 2211334. M.M.M., K.S.B. and O.P are grateful for support from the

Formatted: Not Highlight

Boston College Schiller Institute for Integrated Science and Society Exploratory Collaborative Scholarship grant. M.G. would like to thank the Boston College Cleanroom & Nanofabrication Facility's staff, Stephen Shepard and Dr. Chris Gunderson. M.G. and K.S.B. also thank Dr. Catherine Hoar for her insights on WBE. We would also like to thank Mr. Bryan Horsely, Mr. George Heufelder, and Dr. Sara Wigginton from MASSTC for providing wastewater samples and analysis of their source wastewater contents. M.G. would also like to thank Mark Bukowski from the Veolia wastewater treatment plant for additional wastewater samples. Q.M. and V.B. acknowledge the American Chemical Society Petroleum Research Fund (PRF) 66299-DNI10.

Formatted: Not Highlight

Supporting Information

The supporting information is available free of charge.

Concentration curves for non-pre-linked aptamers (Figure S1); Example Resistance vs. Voltage curves showing Dirac point shifts during experimentation (Figure S2); Reproducibility analysis from over two years of device fabrication (Figure S3); Hill's Equation fitting and LOD calculations (Figure S4); AFM showing graphene height pre- (left) and post- (right) linker+aptamer attachment (Figure S5); Raman measurements of bare graphene, linker+aptamer, and post sensing experiments (Figure S6); Aptamer sequences and sources (S7); Scheme of Pyrene-Aptamer conjugation (Figure S8); Concentration curves using a different wastewater source (Figure S9); Table comparing dynamic range, analysis time, cost for novice user, and LOD in wastewater for all discussed platforms (figure S10

Formatted: Not Highlight

Conflict of Interest Disclosure

Kenneth Stephen Burch reports financial support, equipment, drugs, or supplies, and writing assistance were provided by GRIP Molecular Inc. Kenneth Stephen Burch reports a relationship with GRIP Molecular Inc that includes board membership and equity or stocks. Narendra Kumar reports a

relationship with GRIP Molecular Inc that includes equity or stocks. Kenneth Stephen Burch has a patent pending to Boston College. Micheal Geiwitz has patent pending to Boston College. Stephen Hummel has a patent pending to Boston College. Tim Van Opijnen has a patent pending to Boston College. Narendra Kumar has a patent pending to Boston College. If there are other authors, they declare that they have no known competing financial interests or personal relationships that could have appeared to influence the work reported in this paper.

References

- World Health Organization. The top 10 causes of death. https://www.who.int/news-room/fact-sheets/detail/the-top-10-causes-of-death (accessed 2024-01-10).
- (2) Madhi, S. A.; Polack, F. P.; Piedra, P. A.; Munoz, F. M.; Trenholme, A. A.; Simões, E. A. F.; Swamy, G. K.; Agrawal, S.; Ahmed, K.; August, A.; Baqui, A. H.; Calvert, A.; Chen, J.; Cho, I.; Cotton, M. F.; Cutland, C. L.; Englund, J. A.; Fix, A.; Gonik, B.; Hammitt, L.; Heath, P. T.; de Jesus, J. N.; Jones, C. E.; Khalil, A.; Kimberlin, D. W.; Libster, R.; Llapur, C. J.; Lucero, M.; Pérez Marc, G.; Marshall, H. S.; Masenya, M. S.; Martinón-Torres, F.; Meece, J. K.; Nolan, T. M.; Osman, A.; Perrett, K. P.; Plested, J. S.; Richmond, P. C.; Snape, M. D.; Shakib, J. H.; Shinde, V.; Stoney, T.; Thomas, D. N.; Tita, A. T.; Varner, M. W.; Vatish, M.; Vrbicky, K.; Wen, J.; Zaman, K.; Zar, H. J.; Glenn, G. M.; Fries, L. F. Respiratory Syncytial Virus Vaccination during Pregnancy and Effects in Infants. N. Engl. J. Med. 2020, 383 (5), 426–439.
 https://doi.org/10.1056/NEJMOA1908380/SUPPL_FILE/NEJMOA1908380_DATA-SHARING.PDF.
- (3) Rouzé, A.; Martin-Loeches, I.; Povoa, P.; Makris, D.; Artigas, A.; Bouchereau, M.; Lambiotte, F.; Metzelard, M.; Cuchet, P.; Geronimi, C. B.; Labruyere, M.; Tamion, F.; Nyunga, M.; Luyt, C.-E.; Labreuche, J.; Pouly, O.; Bardin, J.; Saade, A.; Asfar, P.; Baudel, J.-L.; Beurton, A.; Garot, D.; Ioannidou, I.; Kreitmann, L.; Llitjos, J.-F.; Magira, E.; Mégarbane, B.; Meguerditchian, D.; Moglia, E.; Mekontso-Dessap, A.; Reignier, J.; Turpin, M.; Pierre, A.; Plantefeve, G.; Vinsonneau, C.; Floch, P.-E.; Weiss, N.; Ceccato, A.; Torres, A.; Duhamel, A.; Nseir, S. Relationship between SARS-CoV-2 Infection and the Incidence of Ventilator-Associated Lower Respiratory Tract Infections: A European Multicenter Cohort Study. *Intensive Care Med* 2021, 47, 188–198. https://doi.org/10.1007/s00134-020-06323-9.
- (4) Lafond, K. E.; Porter, R. M.; Whaley, M. J.; Suizan, Z.; Ran, Z.; Aleem, M. A.; Thapa, B.; Sar, B.; Proschle, V. S.; Peng, Z.; Feng, L.; Coulibaly, D.; Nkwembe, E.; Olmedo, A.; Ampofo, W.; Saha, S.; Chadha, M.; Mangiri, A.; Setiawaty, V.; Ali, S. S.; Chaves, S. S.; Otorbaeva, D.; Keosavanh, O.; Saleh, M.; Ho, A.; Alexander, B.; Oumzil, H.; Baral, K. P.; Sue Huang, Q.; Adebayo, A. A.; Al-Abaidani, I.; von Horoch, M.; Cohen, C.; Tempia, S.; Mmbaga, V.; Chittaganpitch, M.; Casal, M.; Dang, D. A.; Couto, P.; Nair, H.; Bresee, J. S.; Olsen, S. J.; Azziz-Baumgartner, E.; Pekka Nuorti, J.; Widdowson, M. A.; Flora, M. S.; Wangchuk, S.; Fasce, R. A.; Olivares, M. F.; Qin, Y.; Zheng, J.; Kadjo, H.; Kitoto, L. M.; Ojeda, J.; Armero, J.; Adjabeng, M.; Mena, R.; Rai, S. K.; Broor, S.; Lal, R. B.; Praptiningsih, C. Y.; Susilarini, N. K.; Pangesti, K. N. A.; Sharkas, G.; Emukule, G. O.;

- Kasymbekova, K.; Haddad, N.; Mrad, P.; Aston, S.; Badarch, D.; Upadhyay, S. K.; Wood, T.; Dalhatu, I.; Cabello, M. A.; Tallo, V.; Treurnicht, F.; Venter, M.; Mwakapeje, E.; Praphasiri, P.; Sawatwong, P.; Troeger, C.; Wansaula, Z.; Fierro, M.; Iniguez-Stevens, E.; Nguyen, T. M. T.; Kile, J.; Danielle Iuliano, A.; Rolfes, M.; Mott, J. A.; Moen, A. Global Burden of Influenza-Associated Lower Respiratory Tract Infections and Hospitalizations among Adults: A Systematic Review and Meta-Analysis. *PLOS Med.* **2021**, *18* (3), e1003550. https://doi.org/10.1371/JOURNAL.PMED.1003550.
- (5) Hart, O. E.; Halden, R. U. Computational Analysis of SARS-CoV-2/COVID-19 Surveillance by Wastewater-Based Epidemiology Locally and Globally: Feasibility, Economy, Opportunities and Challenges. Sci. Total Environ. 2020, 730, 138875. https://doi.org/10.1016/j.scitotenv.2020.138875.
- (6) Champredon, D.; Vanrolleghem, P. A. Editorial: Wastewater-Based Epidemiological Surveillance of Respiratory Pathogens. Front. Public Heal. 2023, 11. https://doi.org/10.3389/FPUBH.2023.1328452.
- (7) Peccia, J.; Zulli, A.; Brackney, D. E.; Grubaugh, N. D.; Kaplan, E. H.; Casanovas-Massana, A.; Ko, A. I.; Malik, A. A.; Wang, D.; Wang, M.; Warren, J. L.; Weinberger, D. M.; Arnold, W.; Omer, S. B. Measurement of SARS-CoV-2 RNA in Wastewater Tracks Community Infection Dynamics. *Nat. Biotechnol.* 2020, 38 (10), 1164. https://doi.org/10.1038/S41587-020-0684-Z.
- (8) Karthikeyan, S.; Nguyen, A.; McDonald, D.; Zong, Y.; Ronquillo, N.; Ren, J.; Zou, J.; Farmer, S.; Humphrey, G.; Henderson, D.; Javidi, T.; Messer, K.; Anderson, C.; Schooley, R.; Martin, N. K.; Knight, R. Rapid, Large-Scale Wastewater Surveillance and Automated COVID-19 Cases on a University Campus. Am. Soc. Microbiol. 2021, 6 (4), e00793-21.
- (9) Street, R.; Malema, S.; Mahlangeni, N.; Mathee, A. Wastewater Surveillance for Covid-19: An African Perspective. Sci. Total Environ. 2020, 743, 2018–2020. https://doi.org/10.1016/j.scitotenv.2020.140719.
- (10) Adelodun, B.; Ajibade, F. O.; Ibrahim, R. G.; Bakare, H. O.; Choi, K. S. Snowballing Transmission of COVID-19 (SARS-CoV-2) through Wastewater: Any Sustainable Preventive Measures to Curtail the Scourge in Low-Income Countries? Sci. Total Environ. 2020, 742, 140680. https://doi.org/10.1016/j.scitotenv.2020.140680.
- (11) CDC. *Update on RSV and New Vaccine Recommendation | CDC*. https://www.cdc.gov/respiratory-viruses/whats-new/rsv-update-2023-09-22.html (accessed 2023-11-06).
- (12) Pawar, P. Tracking RSV in Low- and Middle-Income Countries. Nature 2023, 621 (7980), S62–S63. https://doi.org/10.1038/D41586-023-02960-4.
- (13) Lowry, S. A.; Wolfe, M. K.; Boehm, A. B. Respiratory Virus Concentrations in Human Excretions That Contribute to Wastewater: A Systematic Review and Meta-Analysis. *J. Water Health* **2023**, 21 (6), 831–848. https://doi.org/10.2166/WH.2023.057.
- (14) Lorenzo, M.; Picó, Y. Wastewater-Based Epidemiology: Current Status and Future Prospects. Curr. Opin. Environ. Sci. Heal. 2019, 9, 77–84. https://doi.org/10.1016/j.coesh.2019.05.007.
- (15) Leung, N. H. L. Transmissibility and Transmission of Respiratory Viruses. 2021. https://doi.org/10.1038/s41579-021-00535-6.
- (16) Biobot. FAQ Variant Sequencing Biobot Analytics. https://support.biobot.io/hc/en-us/articles/14910772709527-FAQ-Variant-Sequencing (accessed 2023-11-06).

- (17) Adams, G. A Beginner's Guide to RT-PCR, QPCR and RT-QPCR. Biochem. (Lond). 2020, 42 (3), 48–53. https://doi.org/10.1042/BIO20200034.
- (18) Li, Wnkui; Zhang, Ji; Tse, F. L. S. *Handbook of LC-MS Bioanalysis: Best Practices, Experimental Protocols, and ... Google Books*; 2013.
- (19) Komarov, T.; Karnakova, P.; Archakova, O.; Shchelgacheva, D.; Bagaeva, N.; Popova, M.; Karpova, P.; Zaslavskaya, K.; Bely, P.; Shohin, I. Chromatography with Tandem Mass Spectrometry (HPLC-MS/MS) Method for Quantification of Major Development and Validation of a High-Performance Liquid Chromatography with Tandem Mass Spectrometry (HPLC-MS/MS) Method for Quantification of Major Molnupiravir . 2023. https://doi.org/10.3390/biomedicines11092356.
- (20) Massano, M.; Salomone, A.; Gerace, E.; Alladio, E.; Vincenti, M.; Minella, M. Wastewater Surveillance of 105 Pharmaceutical Drugs and Metabolites by Means of Ultra-High-Performance Liquid-Chromatography-Tandem High Resolution Mass Spectrometry. J. Chromatogr. A 2023, 1693, 463896. https://doi.org/10.1016/j.chroma.2023.463896.
- (21) Rainey, A. L.; Liang, S.; Bisesi, J. H.; Sabo-Attwood, T.; Maurelli, A. T. A Multistate Assessment of Population Normalization Factors for Wastewater-Based Epidemiology of COVID-19. *PLoS One* 2023, 18 (4), e0284370. https://doi.org/10.1371/JOURNAL.PONE.0284370.
- (22) Zhang, N.; Gong, Y.; Meng, F.; Bi, Y.; Yang, P.; Wang, F. Virus Shedding Patterns in Nasopharyngeal and Fecal Specimens of COVID-19 Patients. medRxiv 2020, 2020.03.28.20043059. https://doi.org/10.1101/2020.03.28.20043059.
- (23) Wölfel, R.; Corman, V. M.; Guggemos, W.; Seilmaier, M.; Zange, S.; Müller, M. A.; Niemeyer, D.; Jones, T. C.; Vollmar, P.; Rothe, C.; Hoelscher, M.; Bleicker, T.; Brünink, S.; Schneider, J.; Ehmann, R.; Zwirglmaier, K.; Drosten, C.; Wendtner, C. Virological Assessment of Hospitalized Patients with COVID-2019. Nat. 2020 5817809 2020, 581 (7809), 465–469. https://doi.org/10.1038/s41586-020-2196-x.
- (24) Velusamy, K.; Periyasamy, S.; Senthil Kumar, P.; Rangasamy, G.; Mercy, J.; Pauline, N.; Ramaraju, P.; Mohanasundaram, S.; Nguyen Vo, D.-V. Biosensor for Heavy Metal Detection in Wastewater: A Review. Food Chem. Toxicol. 2022, 168, 278–6915. https://doi.org/10.1016/j.fct.2022.113307.
- (25) Kumar, N.; Gray, M.; Ortiz-Marquez, J. C.; Weber, A.; Desmond, C. R.; Argun, A.; Opijnen, T.; Burch, K. S. Detection of a Multi-disease Biomarker in Saliva with Graphene Field Effect Transistors. *Med. DEVICES SENSORS* 2020, e10121. https://doi.org/10.1002/mds3.10121.
- (26) Lu, H. W.; Kane, A. A.; Parkinson, J.; Gao, Y.; Hajian, R.; Heltzen, M.; Goldsmith, B.; Aran, K. The Promise of Graphene-Based Transistors for Democratizing Multiomics Studies. *Biosens*. *Bioelectron.* 2022, 195, 113605. https://doi.org/10.1016/J.BIOS.2021.113605.
- (27) Kumar, N.; Rana, M.; Geiwitz, M.; Khan, N. I.; Catalano, M.; Ortiz-Marquez, J. C.; Kitadai, H.; Weber, A.; Dweik, B.; Ling, X.; van Opijnen, T.; Argun, A. A.; Burch, K. S. Rapid, Multianalyte Detection of Opioid Metabolites in Wastewater. ACS Nano 2022, 16 (3), 3704–3714. https://doi.org/10.1021/acsnano.1c07094.
- (28) Wang, H.; Hao, Z.; Huang, C.; Li, F.; Pan, Y. Monitoring Cd 2+ in Oily Wastewater Using an Aptamer-Graphene Field-Effect Transistor with a Selective Wetting Surface †. 2023. https://doi.org/10.1039/d2na00416j.
- (29) Castro Neto, A. H.; Guinea, F.; Peres, N. M. R.; Novoselov, K. S.; Geim, A. K. The Electronic

- Properties of Graphene. 2009. https://doi.org/10.1103/RevModPhys.81.109.
- (30) Seo, G.; Lee, G.; Kim, M. J.; Baek, S. H.; Choi, M.; Ku, K. B.; Lee, C. S.; Jun, S.; Park, D.; Kim, H. G.; Kim, S. J.; Lee, J. O.; Kim, B. T.; Park, E. C.; Kim, S. II. Rapid Detection of COVID-19 Causative Virus (SARS-CoV-2) in Human Nasopharyngeal Swab Specimens Using Field-Effect Transistor-Based Biosensor. ACS Nano 2020, 14 (4), 5135–5142. https://doi.org/10.1021/ACSNANO.0C02823/ASSET/IMAGES/LARGE/NN0C02823_0006.JPEG.
- (31) Pinto, A. M.; Gonçalves, I. C.; Magalhães, F. D. Graphene-Based Materials Biocompatibility: A Review. Colloids Surfaces B Biointerfaces 2013, 111, 188–202. https://doi.org/10.1016/J.COLSURFB.2013.05.022.
- (32) Khan, N. I.; Song, E. Detection of an IL-6 Biomarker Using a GFET Platform Developed with a Facile Organic Solvent-Free Aptamer Immobilization Approach. Sensors 2021, Vol. 21, Page 1335 2021, 21 (4), 1335. https://doi.org/10.3390/S21041335.
- (33) Fu, W.; Nef, C.; Knopfmacher, O.; Tarasov, A.; Weiss, M.; Calame, M.; Schönenberger, C. Graphene Transistors Are Insensitive to PH Changes in Solution. *Nano Lett.* 2011, 11 (9), 3597–3600. https://doi.org/10.1021/NL201332C/SUPPL_FILE/NL201332C_SI_001.PDF.
- (34) Ping, J.; Vishnubhotla, R.; Vrudhula, A.; Johnson, A. T. C. Scalable Production of High-Sensitivity, Label-Free DNA Biosensors Based on Back-Gated Graphene Field Effect Transistors. ACS Nano 2016, 10 (9), 8700–8704. https://doi.org/10.1021/ACSNANO.6B04110/ASSET/IMAGES/LARGE/NN-2016-04110P_0005.JPEG.
- (35) Kumar, N.; Wang, W.; Ortiz-Marquez, J. C.; Catalano, M.; Gray, M.; Biglari, N.; Hikari, K.; Ling, X.; Gao, J.; van Opijnen, T.; Burch, K. S. Dielectrophoresis Assisted Rapid, Selective and Single Cell Detection of Antibiotic Resistant Bacteria with G-FETs. *Biosens. Bioelectron.* 2020, 156 (February), 112123. https://doi.org/10.1016/j.bios.2020.112123.
- (36) Urmann, K.; Modrejewski, J.; Scheper, T.; Walter, J. G. Aptamer-Modified Nanomaterials: Principles and Applications. *BioNanoMaterials* 2017, 18 (1–2), 20160012. https://doi.org/10.1515/BNM-2016-0012/ASSET/GRAPHIC/J BNM-2016-0012 FIG 001.JPG.
- (37) Wu, Y.; Zhan, S.; Wang, L.; Zhou, P. Selection of a DNA Aptamer for Cadmium Detection Based on Cationic Polymer Mediated Aggregation of Gold Nanoparticles. *Analyst* 2014, 139 (6), 1550–1561. https://doi.org/10.1039/C3AN02117C.
- (38) Jones, S.; Daley, D. T. A.; Luscombe, N. M.; Berman, H. M.; Thornton, J. M. Protein–RNA Interactions: a Structural Analysis. *Nucleic Acids Res.* 2001, 29 (4), 943. https://doi.org/10.1093/NAR/29.4.943.
- (39) Qian, S.; Chang, D.; He, S.; Li, Y. Aptamers from Random Sequence Space: Accomplishments, Gaps and Future Considerations. *Anal. Chim. Acta* 2022, 1196, 339511. https://doi.org/10.1016/J.ACA.2022.339511.
- (40) Zhou, J.; Rossi, J. Aptamers as Targeted Therapeutics: Current Potential and Challenges. Nat. Rev. Drug Discov. 2017, 16 (3), 181. https://doi.org/10.1038/NRD.2016.199.
- (41) Shiratori, I.; Akitomi, J.; Boltz, D. A.; Horii, K.; Furuichi, M.; Waga, I. Selection of DNA Aptamers That Bind to Influenza A Viruses with High Affinity and Broad Subtype Specificity. *Biochem. Biophys. Res. Commun.* **2014**, *443* (1), 37–41. https://doi.org/10.1016/j.bbrc.2013.11.041.

- (42) Percze, K.; Szakács, Z.; Scholz, É.; András, J.; Szeitner, Z.; Van Den Kieboom, C. H.; Ferwerda, G.; De Jonge, M. I.; Gyurcsányi, R. E.; Mészáros, T. Aptamers for Respiratory Syncytial Virus Detection OPEN. 2017. https://doi.org/10.1038/srep42794.
- (43) Zhang, Y.; Juhas, M.; Kwok, C. K. Aptamers Targeting SARS-COV-2: A Promising Tool to Fight against COVID-19. 2022. https://doi.org/10.1016/j.tibtech.2022.07.012.
- (44) Szunerits, S.; Rodrigues, T.; Bagale, R.; Happy, H.; Boukherroub, R.; Knoll, W. Graphene-Based Field-Effect Transistors for Biosensing: Where Is the Field Heading To? *Anal. Bioanal. Chem.* **2023**, 1–14. https://doi.org/10.1007/S00216-023-04760-1/TABLES/1.
- (45) Wu, G.; Tang, X.; Meyyappan, M.; Wai Chiu Lai, K. Doping Effects of Surface Functionalization on Graphene with Aromatic Molecule and Organic Solvents. Appl. Surf. Sci. 2017, 425, 713–721. https://doi.org/10.1016/j.apsusc.2017.07.048.
- (46) Gray, M. J.; Kumar, N.; O'Connor, R.; Hoek, M.; Sheridan, E.; Doyle, M. C.; Romanelli, M. L.; Osterhoudt, G. B.; Wang, Y.; Plisson, V.; Lei, S.; Zhong, R.; Rachmilowitz, B.; Zhao, H.; Kitadai, H.; Shepard, S.; Schoop, L. M.; Gu, G. D.; Zeljkovic, I.; Ling, X.; Burch, K. S. A Cleanroom in a Glovebox. Rev. Sci. Instrum. 2020, 91 (7), 073909. https://doi.org/10.1063/5.0006462.
- (47) Huang, M. H.; Li, Y. M.; Gu, G. W. Chemical Composition of Organic Matters in Domestic Wastewater. *Desalination* **2010**, *262* (1–3), 36–42. https://doi.org/10.1016/j.desal.2010.05.037.
- (48) Stern, E. Label-Free Sensing with Semiconducting Nanowires. 2007.
- (49) Fujii, S.; Kasuya, M.; Kurihara, K. Characterization of Platinum Electrode Surfaces by Electrochemical Surface Forces Measurement. J. Phys. Chem. C 2017, 121 (47), 26406–26413. https://doi.org/10.1021/ACS.JPCC.7B09301.
- (50) Gosling, J. H.; Makarovsky, O.; Wang, F.; Cottam, N. D.; Greenaway, M. T.; Patanè, A.; Wildman, R. D.; Tuck, C. J.; Turyanska, L.; Fromhold, T. M. Universal Mobility Characteristics of Graphene Originating from Charge Scattering by Ionised Impurities. *Commun. Phys.* 2021, 4 (1). https://doi.org/10.1038/s42005-021-00518-2.
- (51) Goutelle, S.; Maurin, M.; Rougier, F.; Barbaut, X.; Bourguignon, L.; Ducher, M.; Maire, P. The Hill Equation: A Review of Its Capabilities in Pharmacological Modelling. *Fundamental and Clinical Pharmacology*, 2008, pp 633–648. https://doi.org/10.1111/j.1472-8206.2008.00633.x.
- (52) Belter, M.; Sajnóg, A.; Barałkiewicz, D. Over a Century of Detection and Quantification Capabilities in Analytical Chemistry-Historical Overview and Trends. 2014. https://doi.org/10.1016/j.talanta.2014.05.018.
- (53) Hsu, S. Y.; Bayati, M.; Li, C.; Hsieh, H. Y.; Belenchia, A.; Klutts, J.; Zemmer, S. A.; Reynolds, M.; Semkiw, E.; Johnson, H. Y.; Foley, T.; Wieberg, C. G.; Wenzel, J.; Johnson, M. C.; Lin, C. H. Biomarkers Selection for Population Normalization in SARS-CoV-2 Wastewater-Based Epidemiology. Water Res. 2022, 223, 118985. https://doi.org/10.1016/J.WATRES.2022.118985.
- (54) Huang, P. J. J.; Liu, J. Selection of Aptamers for Sensing Caffeine and Discrimination of Its Three Single Demethylated Analogues. Anal. Chem. 2022, 94 (7), 3142–3149. https://doi.org/10.1021/ACS.ANALCHEM.1C04349/ASSET/IMAGES/LARGE/AC1C04349_0006.JPE G.
- (55) Ke, Z.; Oton, J.; Qu, K.; Cortese, M.; Zila, V.; McKeane, L.; Nakane, T.; Zivanov, J.; Neufeldt, C. J.;

- Cerikan, B.; Lu, J. M.; Peukes, J.; Xiong, X.; Kräusslich, H. G.; Scheres, S. H. W.; Bartenschlager, R.; Briggs, J. A. G. Structures and Distributions of SARS-CoV-2 Spike Proteins on Intact Virions. *Nat.* 2020 5887838 2020, 588 (7838), 498–502. https://doi.org/10.1038/s41586-020-2665-2.
- (56) Einav, T.; Gentles, L. E.; Bloom, J. D. SnapShot: Influenza by the Numbers. Cell 2020, 182. https://doi.org/10.1016/j.cell.2020.05.004.
- (57) Lores, E. M.; Pennock, J. R. The Effect of Salinity on Binding of Cd, Cr, Cu and Zn to Dissolved Organic Matter. Chemosphere 1998, 37 (5), 861–874. https://doi.org/10.1016/S0045-6535(98)00090-3.
- (58) Biobot. FAQ Technical Questions: Results Biobot Analytics. https://support.biobot.io/hc/en-us/articles/360052012934-FAQ-Technical-Questions-Results (accessed 2023-11-06).
- (59) Sender, R.; Bar-On, Y. M.; Gleizer, S.; Bernsthein, B.; Flamholz, A.; Phillips, R.; Milo, R. The Total Number and Mass of SARS-CoV-2 Virions. medRxiv 2020. https://doi.org/10.1101/2020.11.16.20232009.
- (60) Heijnen, L.; Medema, G. Surveillance of Influenza A and the Pandemic Influenza A (H1N1) 2009 in Sewage and Surface Water in the Netherlands. 2011. https://doi.org/10.2166/wh.2011.019.
- (61) Ahmed, W.; Bivins, A.; Stephens, M.; Metcalfe, S.; Smith, W. J. M.; Sirikanchana, K.; Kitajima, M.; Simpson, S. L. Occurrence of Multiple Respiratory Viruses in Wastewater in Queensland, Australia: Potential for Community Disease Surveillance. Sci. Total Environ. 2023, 864, 161023. https://doi.org/10.1016/j.scitotenv.2022.161023.
- (62) Ahmed, W.; Smith, W. J. M.; Metcalfe, S.; Jackson, G.; Choi, P. M.; Morrison, M.; Field, D.; Gyawali, P.; Bivins, A.; Bibby, K.; Simpson, S. L. Comparison of RT-QPCR and RT-DPCR Platforms for the Trace Detection of SARS-CoV-2 RNA in Wastewater. ACS ES T Water 2022, 2 (11), 1871– 1880. https://doi.org/10.1021/ACSESTWATER.1C00387/ASSET/IMAGES/LARGE/EW1C00387_0001.JPEG
- (63) Jones, D. L.; Baluja, M. Q.; Graham, D. W.; Corbishley, A.; McDonald, J. E.; Malham, S. K.; Hillary, L. S.; Connor, T. R.; Gaze, W. H.; Moura, I. B.; Wilcox, M. H.; Farkas, K. Shedding of SARS-CoV-2 in Feces and Urine and Its Potential Role in Person-to-Person Transmission and the Environment-Based Spread of COVID-19. Sci. Total Environ. 2020, 749, 141364. https://doi.org/10.1016/J.SCITOTENV.2020.141364.
- (64) Pan, Y.; Zhang, D.; Yang, P.; Poon, L. L. M.; Wang, Q. Viral Load of SARS-CoV-2 in Clinical Samples. Lancet. Infect. Dis. 2020, 20 (4), 411. https://doi.org/10.1016/S1473-3099(20)30113-4.
- (65) Dollman, N. L.; Griffin, J. H.; Downard, K. M. Detection, Mapping, and Proteotyping of SARS-CoV-2 Coronavirus with High Resolution Mass Spectrometry. ACS Infect. Dis. 2020, 6 (12), 3269–3276. https://doi.org/10.1021/ACSINFECDIS.0C00664.
- (66) Nikolaev, E. N.; Indeykina, M. I.; Brzhozovskiy, A. G.; Bugrova, A. E.; Kononikhin, A. S.; Starodubtseva, N. L.; Petrotchenko, E. V.; Kovalev, G. I.; Borchers, C. H.; Sukhikh, G. T. Mass-Spectrometric Detection of SARS-CoV-2 Virus in Scrapings of the Epithelium of the Nasopharynx of Infected Patients via Nucleocapsid N Protein. J. Proteome Res. 2020, 19 (11), 4393–4397. https://doi.org/10.1021/ACS.JPROTEOME.0C00412/ASSET/IMAGES/MEDIUM/PR0C00412_0003. GIF.

- (67) Bojórquez-Velázquez, E.; Llamas-García, M. L.; Elizalde-Contreras, J. M.; Zamora-Briseño, J. A.; Ruiz-May, E. Mass Spectrometry Approaches for SARS-CoV-2 Detection: Harnessing for Application in Food and Environmental Samples. *Viruses 2022, Vol. 14, Page 872* 2022, 14 (5), 872. https://doi.org/10.3390/V14050872.
- (68) Huerta-Fontela, M.; Galceran, M. T.; Ventura, F. Ultraperformance Liquid Chromatography Tandem Mass Spectrometry Analysis of Stimulatory Drugs of Abuse in Wastewater and Surface Waters. Anal. Chem. 2007, 79 (10), 3821–3829. https://doi.org/10.1021/AC062370X/ASSET/IMAGES/LARGE/AC062370XF00003.JPEG.
- (69) Peng, J.; Sun, J.; Yang, M. I.; Gibson, R. M.; Arts, E. J.; Olabode, A. S.; Poon, A. F. Y.; Wang, X.; Wheeler, A. R.; Edwards, E. A.; Peng, H. Early Warning Measurement of SARS-CoV-2 Variants of Concern in Wastewaters by Mass Spectrometry. *Environ. Sci. Technol. Lett.* 2022, 9 (7), 638–644. https://doi.org/10.1021/ACS.ESTLETT.2C00280/ASSET/IMAGES/LARGE/EZ2C00280 0003.JPEG.
- (70) Rames, E. K.; Macdonald, J. Rapid Assessment of Viral Water Quality Using a Novel Recombinase Polymerase Amplification Test for Human Adenovirus. Appl. Microbiol. Biotechnol. 2019, 103 (19), 8115–8125. https://doi.org/10.1007/S00253-019-10077-W/TABLES/2.

For Table of Contents Only

